Spectral analysis of electron transfer kinetics. I. Symmetric reactions

Jianshu Cao[a] and Younjoon Jung
Department of Chemistry, Massachusetts Institute of Technology, Cambridge, Massachusetts 02139

(Received 20 August 1999; accepted 13 December 1999)

A spectral analysis method is proposed to characterize multiple time scales in electron transfer processes, including vibrational relaxation, electronic coherence, activated curve crossing, or barrier crossing. Within this unified framework, observed rate behavior, biexponential and multiexponential decay, and population recurrences and oscillations are different components of the same kinetic spectrum; thus, several existing theoretical models, developed for limiting cases of electron transfer, can be analyzed, tested, and extended. In particular, the rate constant extracted from the analysis does not saturate as the electronic coupling increases but shows a crossover from the nonadiabatic to adiabatic limits, and the kinetic spectrum in the large coupling regime reveals the nature of the localization–delocalization transition as the consequence of two competing mechanisms. Though the analysis is presented in the context of electron transfer, this approach provides a different perspective for understanding dissipative dynamics and hence can be applied to study condensed-phase laser spectroscopy, quantum coherence control, energy transfer, and other charge transfer processes. © *2000 American Institute of Physics.* [S0021-9606(00)50410-3]

I. INTRODUCTION

Multiple time scales characterize many complex dynamic systems, especially chemical and biological systems. A classical example is electron transfer processes,[1,2] which involve time scales associated with solvent relaxation, electronic coherence, and activated curve crossing or barrier crossing. Recent studies of electron transfer processes have revealed rich kinetic behavior, which cannot be described by the classical Marcus electron transfer theory. For example, the increase of electronic coupling constants leads to a transition from nonadiabatic to adiabatic electron transfer, and this transition is influenced by the dynamic nature of the solvent. Further, electron transfer in mixed-valence molecules and other strongly-coupled electronic systems demonstrates underdamped oscillations. The goal of this article is to illustrate a spectral method to analyze various time scales in electron transfer systems showing that experimentally observed rate behavior, biexponential decay, population recurrences, and oscillations are simply components of the same kinetic spectrum.

Several kinetic regimes of electron transfer have been modeled and calculated. An important feature of electron transfer is the crossover from the nonadiabatic regime in Fig. 1(a) ($V \ll k_B T$) to the adiabatic regime in Fig. 1(b) ($V > k_B T$), due to the increase of the electronic coupling constant V. At high temperature, the Landau–Zener expression allows us to interpolate rate constants between these two limits.[3,4] At low temperature, rate is enhanced by quantum tunneling effects,[5] and a nonadiabatic instanton theory has been developed to account for the crossover in the quantum regime.[6] Further, when the coupling constant (V) approaches half the reorganization energy ($\lambda/2$) as in Fig. 1(c), there is a transition in the electronic state from the localized to the delocalized regime.[7] Similar transitions have been predicted for two-level systems coupled to low temperature phonon modes.[8–10] It has recently been suggested that the delocalized electronic state is responsible for population oscillations observed in mixed-valence systems.[11]

As for all statistical arguments, thermal rate theories are based on the assumption that solvent relaxation is instantaneous so that thermal equilibrium is maintained at the transition state (or equivalently, the crossing point in curve crossing). In reality, the finite response time of solvents imposes an upper-bound for the measured electron transfer rate. Treating solvent relaxation as a competing mechanism, one can invoke the stable state picture to construct a general expression for observed electron transfer rate, $1/k = 1/k_{\mathrm{ET}} + 1/k_D$,[12,13] where k_{ET} is the thermal rate for electron transfer and k_D is the spatial-diffusion-limited reaction rate. Rigorously, this relation holds only in the nonadiabatic regime with $k_{\mathrm{ET}} = k_{\mathrm{NA}}$.[14] As seen from the above discussions, existing models apply to limiting cases of electron transfer; hence, the spectral method we propose in this article will provide a unified approach to analyze, test, and extend existing rate theories.

The article is organized as follows: the kinetic spectral method is introduced in Sec. II, the two-state diffusion model for electron transfer is analyzed in Sec. III, numerical results of spectral analysis are then presented in Sec. IV, and finally a summary in Sec. V concludes the article.

II. SPECTRAL ANALYSIS METHOD

Simply put, spectral analysis is to treat dissipative dynamics as an eigenvalue problem. In general, the evolution of a dynamic system follows the equation of motion

$$\dot{\rho}(t) = \mathcal{L}\rho(t), \tag{1}$$

[a]Electronic mail: jianshu@mit.edu

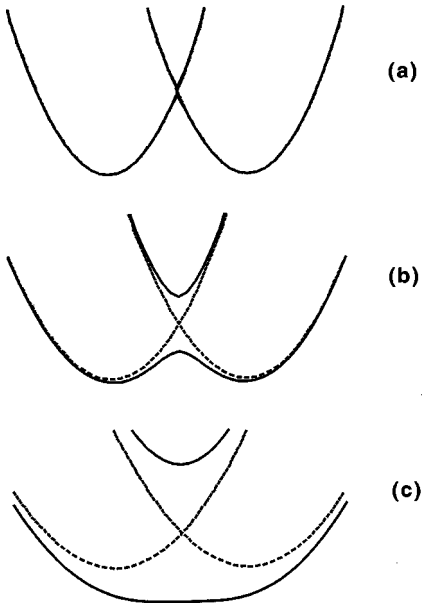

FIG. 1. Adiabatic potential surfaces (solid curves) vs. diabatic potential surfaces (dotted curves). The diabatic Hamiltonians are $H_1(E)=(E+\lambda)^2/(4\lambda)$ and $H_2(E)=(E-\lambda)^2/(4\lambda)$ with $\beta\lambda=8$. The three diagrams represent three kinetic regimes: (a) $\beta V=0.1$, (nonadiabatic); (b) $\beta V=1.0$, (adiabatic); (c) $\beta V=4.0$, (delocalized state). For all the figures in the article time and energy variables are scaled by the thermal energy β, and $\hbar$ is taken as unity.

where $\rho(t)$ is the distribution function in multidimensional space, and $\mathcal{L}$ is the Liouville operator. For classical systems, Eq. (1) takes the form of the Boltzmann equation or the Fokker–Planck equation. For quantum systems, Eq. (1) can be formulated with influence functionals, semiclassical approximations, and Bloch–Redfield equations. For a dissipative system, the Liouville operator has a non-Hermitian part, which is responsible for irreversible mechanisms in the process. The non-Hermitian Liouville operator, $\mathcal{L}$, can then be diagonalized, giving

$$\phi_n^L \mathcal{L} \phi_n^R = Z_n, \tag{2}$$

where ϕ^L and ϕ^R are the left and right eigenvectors, respectively, and Z is the corresponding eigenvalue. Just as eigenstates of the Schrödinger equation are dynamic normal modes, ϕ can be understood as kinetic normal modes, or dissipative eigenstates, with $\mathcal{R}Z$ the decay rate and $\mathcal{J}Z$ the oscillation frequency. Thus, the set of eigensolutions $\{Z_n, \phi_n\}$ forms the kinetic spectrum, which completely characterizes the intrinsic time scales of a dissipative system.

Formally, the time evolution can be expanded as

$$\rho(t)=\sum_{n=0}^{\infty} e^{Z_n t} |\phi_n^R\rangle\langle\phi_n^L|\rho(0)\rangle, \tag{3}$$

where $\rho(0)$ is the initial distribution function. Based on simple physical considerations, the real part of any eigenvalue must be less or equal to zero, $\mathcal{R}Z_1 \leqslant 0$, and the ground state is thermal equilibrium with zero eigenvalue, $Z_0=0$. If the first nonzero eigenvalue is well-separated from other nonzero eigenvalues, then the long-time behavior is dominated by exponential decay with rate constant $k=-\mathcal{R}Z_1$. This argument allows us to extract rate constants for the complete range of parameter space. In a similar fashion, biexponential decay, multiexponential decay, and damped oscillations can also be predicted and analyzed.

Furthermore, observed kinetics can be predicted by identifying the kinetic eigenstate corresponding to the experimental time scale, and the initial preparation in ultrafast experiments can be interpreted as projections to different kinetic eigenstates. This is particularly useful for studying coherent excitation[15] and laser spectroscopy[16] in condensed phase systems, which can now be treated in the same fashion as gas phase systems. For example, relationships between photoexcitation and kinetic modes can be established, which can be used as a guide for the design of laser pulses for selective photochemistry.

Earlier, the kinetic spectral method has been used to study one-dimensional and two-dimensional diffusive barrier crossing.[17,18] Cukier and co-workers have also applied the method to calculate electron transfer rate constants in the small electronic coupling regime.[19] The goal of this study is to use the kinetic method to explore various kinetic regimes of electron transfer.

III. ANALYSIS OF ELECTRON TRANSFER RATE

A. Two-state diffusion equation

Since most chemical and biological processes take place in over-damped solvent environments, electron transfer processes can be modeled as two-state dynamics in Debye solvents. Taking the over-damped limit of two-state quantum dissipative equations,[14,20,16] we obtain a set of classical diffusion equations for two-coupled surfaces,

$$\dot{\rho}_1=\mathcal{L}_1\rho_1 - iV(\rho_{12}-\rho_{21}), \tag{4a}$$

$$\dot{\rho}_2=\mathcal{L}_2\rho_2 + iV(\rho_{12}-\rho_{21}), \tag{4b}$$

$$\dot{\rho}_{12}=\mathcal{L}_{12}\rho_{12} - i\omega_{12}\rho_{12} + iV(\rho_1-\rho_2), \tag{4c}$$

where $\mathcal{L}_{12}=(\mathcal{L}_1+\mathcal{L}_2)/2$, $\hbar\omega_{12}=U_1(E)-U_2(E)$, and $\mathcal{L}$ is 1D Fokker–Planck operator $\mathcal{L}\rho=D_E[\partial^2/\partial E^2 + \beta\partial/\partial E U'(E)]\rho$, defined on potential surface U_1 or U_2, respectively. Here, the stochastic variable E is the electronic energy, which is a function of solvent configuration: the large number of degrees of freedom in the solvent defines a Gaussian process, thus giving $U_1=(E+\lambda)^2/(4\lambda)$ and $U_2=(E-\lambda)^2/(4\lambda)+\epsilon$, with λ the reorganization energy and ϵ the free energy bias; D_E is the energy diffusion constant, $D_E=\Omega\alpha$, where Ω is the solvent relaxation rate and $\alpha=2k_BT\lambda$ is the mean-square fluctuation of the energy. This set of equations is also known as the stochastic Liouville equation, which was first used by Zusman for studying dynamic solvent effects on electron transfer in the nonadiabatic limit.

It should be noted that the two-state diffusion equations describe mixed classical-quantum dynamics, where the solvent is treated classically and the electronic coupling is treated quantum mechanically. In the kinetic regimes of interest, the two-state diffusion equations have a well-defined eigenstructure, which allows us to extract rate constants and to characterize kinetic mechanisms. However, in general, Newtonian dynamics is intrinsically not an eigenvalue prob-

lem, unless classical motions become stochastic in the presence of strong friction. On the other hand, since quantum dynamics described by the Schrödinger equation is dictated by the underlying eigenstructure, one may speculate that quantum dissipative dynamics can also be posed as an eigenvalue problem and the kinetic spectral analysis can be applicable. This direction will be explored in the future.

B. Adiabatic limit

To study the adiabatic limit in the activated regime, we diagonalize the two-state system at each value of E and transform the two-state diffusion equations to the adiabatic representation. Then, the two-state dynamics is simplified to diffusion on a single potential surface, $\dot{\rho}=\mathcal{L}\rho=D_E[\partial^2/\partial E^2+\beta\partial/\partial E U_A'(E)]\rho$, where U_A is the lower adiabatic potential surface defined by

$$U_A(E)=\frac{E^2+\lambda^2}{4\lambda}-\frac{1}{2}\sqrt{E^2+4V^2}. \tag{5}$$

Because the 1D Fokker–Planck operator $\mathcal{L}$ is Hermitian, the adiabatic diffusion equation has a set of real eigenvalues, $\{Z_n\}$, and the first nonzero eigenvalue defines the spatial-diffusion-limited rate, $k_D=-Z_1$. For the symmetric double well in Fig. 1, the diffusion rate is evaluated by the stationary-flux method,[21]

$$k_D^{-1}=\frac{1}{\Omega\alpha}\int_{-\infty}^{E_c}e^{\beta U_A(E_1)}\int_{-\infty}^{E_1}e^{\beta U_A(E_2)}dE_1dE_2, \tag{6}$$

where E_c is the transition state ($E_c=0$ for the symmetric case). In the large-coupling regime ($\beta\lambda>\beta V>1$), both the well and the barrier are nearly quadratic and the steepest descent evaluation of Eq. (6) leads to

$$k_D=\frac{\Omega}{\pi}\sqrt{\frac{\lambda}{2V}}e^{-\beta(\lambda/4-V)}, \tag{7}$$

which is the strong-friction limit of the Kramers rate. The adiabatic limit of electron transfer has been obtained previously within the framework of transition state theory for an arbitrary solvent spectrum.[22] In the small-coupling regime ($\beta V<1$), the barrier becomes a cusp-ed potential and the dominant contribution can be evaluated by linear expansion at the crossing point to give

$$k_D=\Omega\lambda\rho(\lambda+\epsilon), \tag{8}$$

where $\rho(E)=\exp[-(E)^2/2\alpha]/\sqrt{2\pi\alpha}$ is the equilibrium probability distribution.

C. Nonadiabatic limit

In the nonadiabatic limit, curve crossing is confined to a small region that can be approximated by a delta function, $\delta(E-E_c)$, at the crossing point E_c. The crossing point (i.e., transition state), $E_c=\epsilon$, is determined from $U_2(E_c)=U_1(E_c)$. A rigorous derivation leads to the nonlocalized curve crossing, which reduces to the delta function under certain conditions.[23] Formally, the off-diagonal element ρ_{12} can be integrated to yield

$$\rho_{12}\approx\frac{1}{\omega_{12}+i\epsilon}(\rho_1-\rho_2), \tag{9}$$

with $\epsilon=0^+$; therefore, electron transfer is described as diffusion on the two diabatic surfaces with population exchange at the crossing point,

$$\dot{\rho}_1=\mathcal{L}_1\rho_1-\eta\delta(E-E_c)(\rho_1-\rho_2), \tag{10a}$$

$$\dot{\rho}_2=\mathcal{L}_2\rho_2+\eta\delta(E-E_c)(\rho_1-\rho_2), \tag{10b}$$

where the coefficient for nonadiabatic transition is $\eta=2\pi V^2/\hbar$. For unbiased electron transfer ($\epsilon=0$), a symmetric eigenfunction, $\psi_g=(\sqrt{\rho_1}|1\rangle+\sqrt{\rho_2}|2\rangle)/\sqrt{2}$, can be constructed for the ground state equilibrium distribution, and an antisymmetric eigenfunction, $\psi_u=(\sqrt{\rho_1}|1\rangle-\sqrt{\rho_2}|2\rangle)/\sqrt{2}$, can be constructed as the first excited state. Here, $\rho_1=\rho(E+\lambda)$ and $\rho_2=\rho(E-\lambda)$, with ρ being the equilibrium distribution. Then, to first-order perturbation, the shift in the eigenvalue for ψ_u leads to an estimation for the nonadiabatic rate,

$$k_{\mathrm{NA}}=-Z=-\langle\psi_u|\mathcal{L}'|\psi_u\rangle=2\eta\rho(\lambda), \tag{11}$$

which is the celebrated Marcus rate expression.

To incorporate solvent effects, the higher-order perturbation terms can be evaluated by applying the Goldstone's theorem[24] to obtain an expansion for the eigenvalue Z_1,

$$Z=\langle\psi_u|\mathcal{L}'\sum_{m=0}^{\infty}\left(-\frac{1}{\mathcal{L}_0}\mathcal{L}'\right)^m|\psi_u\rangle, \tag{12}$$

where $\mathcal{L}_0=\mathcal{L}_1|1\rangle\langle 1|+\mathcal{L}_2|2\rangle\langle 2|$ is the unperturbed operator and $\mathcal{L}'=-\eta\delta(E-E_c)(|1\rangle\langle 1|+|2\rangle\langle 2|-|1\rangle\langle 2|-|2\rangle\langle 1|)$ is the perturbation. For a delta function perturbation, Eq. (12) can be explicitly evaluated

$$\begin{aligned}-Z&=2\eta\rho(\lambda)+2\eta^2\rho(\lambda)\sum_{n\neq 0}\frac{\rho_n(\lambda)}{Z_n^{(0)}}\\&\quad+2\eta^3\rho(\lambda)\sum_{n\neq 0}\frac{\rho_n(\lambda)}{Z_n^{(0)}}\sum_{m\neq 0}\frac{\rho_m(\lambda)}{Z_m^{(0)}}+\cdots\\&=\frac{2\eta\rho(\lambda)}{1-\eta\Sigma_{n\neq 0}\rho_n(\lambda)/Z_n^{(0)}},\end{aligned} \tag{13}$$

where $Z_n^{(0)}$ is the unperturbed eigenvalue of ρ_n, the nth eigensolution of odd parity. The infinite series in Eq. (13) can be resumed to yield the diffusion-limited rate expression

$$\frac{1}{k}=\frac{1}{k_{\mathrm{NA}}}+\frac{1}{k_D}, \tag{14}$$

where k_{NA} is given in Eq. (11), k_D is the diffusion rate defined by

$$\begin{aligned}\frac{1}{k_D}&=-\frac{1}{\rho(\lambda)}\sum_{n\neq 0}\frac{\rho_n(\lambda)}{Z_n^{(0)}}\\&=\frac{1}{\rho(\lambda)}\int_0^{\infty}[G(\lambda,t)-G(\lambda,\infty)]dt,\end{aligned} \tag{15}$$

and $G(E,t)$ is the survival probability

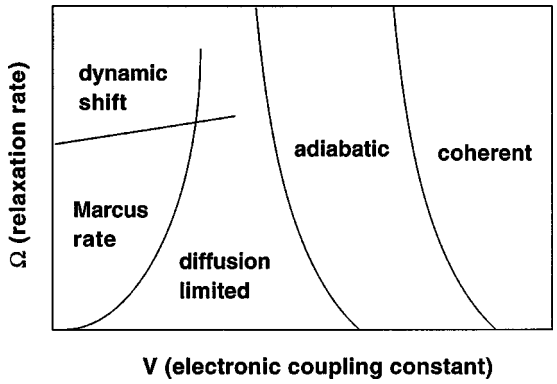

FIG. 2. The validity of the Marcus rate theory is illustrated by identifying various kinetic regime in parameter space.

$$G(E,t)=\sum_n \rho_n(E)e^{Z_n^0 t}$$

$$=\frac{1}{\sqrt{[1-C^2(t)]2\pi\alpha}}\exp\left[-\frac{E^2}{2\alpha}\frac{1-C(t)}{1+C(t)}\right], \quad (16)$$

with $C(t)=e^{-\Omega t}$ and $G(E,\infty)=\rho(E)$. In the activated regime ($\beta\lambda>1>\beta V$), k_D can be approximated by $k_D \approx \Omega\lambda\rho(\lambda)$, which recovers k_D in Eq. (8) for a cusp-ed barrier. Equation (14) is equivalent to the nonperturbative weak-coupling rate formula first derived by Zusman using Laplace transformation[14] and later by several authors.[20,13,25–28] A similar expression for asymmetric electron transfer is derived in the Appendix.

D. Validity of Marcus rate expression

There are three possible factors which may cause deviations from equilibrium rate theory: solvent diffusion, adiabatic crossing, and dynamic solvation. As shown in Fig. 2, we can establish domains in parameter space where each of these factors becomes appreciable and where Marcus electron transfer rate theory can be violated.

1. Solvent diffusion

As demonstrated in Sec. III, the observed rate is the combined result of nonadiabatic curve crossing and diffusive solvent relaxation. According to Eq. (14), the solvent diffusion effect can be ignored when $k_D \gg k_{\mathrm{NA}}$, i.e.,

$$2\pi V^2 < \lambda\Omega\hbar, \quad (17)$$

which imposes a strong restriction on the use of the original Marcus rate expression.

2. Adiabatic crossing

To examine the weak-coupling limit of the two-state diffusion equations, we rewrite the equation for electronic coherence term, Eq. 4(c), in dimensionless unit, giving

$$\frac{d\rho_{12}}{d\bar{t}}=\mathcal{L}_{12}(\bar{E})\rho_{12}-i\frac{\omega_{12}}{D_E^{1/3}}\rho_{12}+i\frac{V}{D_E^{1/3}}(\rho_1-\rho_2), \quad (18)$$

where $\bar{t}=tD_E^{1/3}$ and $\bar{E}=E/D_E^{1/3}$. Then, the off-diagonal term varies on the characteristic scale of $D_E^{1/3}$, and the weak coupling limit can be established as

$$V \ll D_E^{1/3}=(\alpha\Omega)^{1/3}, \quad (19)$$

which has been obtained earlier by several authors. In addition, the strong condition for adiabatic transfer can be estimated as

$$V>\beta^{-1}, \quad (20)$$

where the upper electronic surface is not thermally accessible and the reaction takes place on the lower adiabatic surface, as in the case discussed in Sec. III B.

3. Dynamic solvation

To understand the dynamic effect induced by the solvent, we start with the Golden-rule expression

$$k=\frac{V^2}{\hbar}\int_{-\infty}^{\infty}d\tau\langle e^{i\tau\epsilon-i\phi(\tau)}\rangle_{\mathrm{solvent}}, \quad (21)$$

where the stochastic phase is $\phi(\tau)=\int_0^\tau E(s)ds$. This Golden-rule approach follows stochastic line-shape theory by Kubo, and reduces to the Marcus rate expression in the inhomogeneous limit (i.e., the static solvent limit) under the condition

$$\Omega^2 < \alpha = 2\lambda k_B T. \quad (22)$$

Similar to the Stokes shift and motional narrowing in line-shape theory, when Eq. (22) is not satisfied, the dynamic nature of the solvent leads to deviations from the Marcus rate, which become significant in the inverted regime. For example, the reorganization energy in the Marcus theory describes the solvation of a static solvent, so dynamic solvation reduces the reorganization energy, thus increasing the rate constant in the normal regime and decreasing the energy bias for barrierless transfer. A more rigorous account of dynamic solvent effects starting from the two-state diffusion equations has been shown by Jung *et al.*[23]

As pointed out by Hynes,[13] typical cases of outer-sphere electron transfer reactions fall in the small-coupling (1–10 cm^{-1}) or weak-adiabatic (10–100 cm^{-1}) regime, so that Marcus rate theory can qualitatively explain experimental measurements. For a typical solvent with ($\Omega=1-10\,\mathrm{ps}^{-1}$),[29] the solvent diffusion effect is the limiting mechanism in the rate process except in the inverted regime where the dynamic solvation effect becomes appreciable. It should be emphasized that the two-state diffusion model in this article describes electron transfer in overdamped solvents, where the Landau–Zener expression is not applicable. More general cases of electron transfer have been discussed by Wolynes.[3]

IV. NUMERICAL RESULTS

In the broad range of parameter space beyond the adiabatic and nonadiabatic limits, eigensolutions to the two-state diffusion equation provide a reliable means to extract electron transfer rate constants. As an example, electron transfer rate constants are plotted in Fig. 3 as functions of the elec-

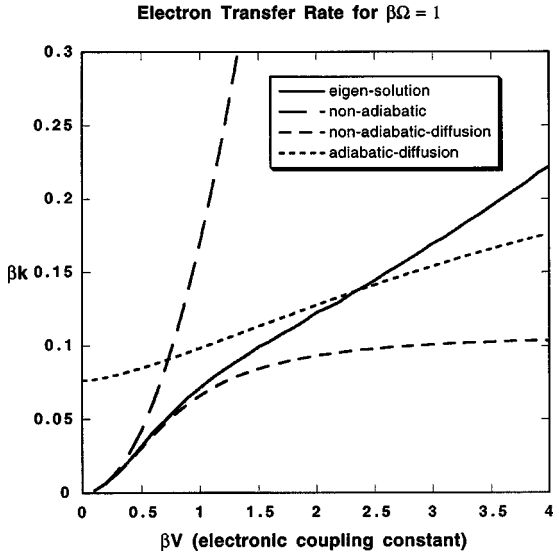

FIG. 3. A plot of electron transfer rate constants as functions of the electronic coupling constant βV for $\beta\lambda=8$ and $\beta\Omega=1$. The long-dashed curve is the Marcus rate, the dashed curve is the diffusion-limited nonadiabatic rate (i.e., the Zusman rate), the short-dashed curve is the adiabatic diffusion rate, and the solid curve is the eigenvalue solution to the two-state diffusion equation.

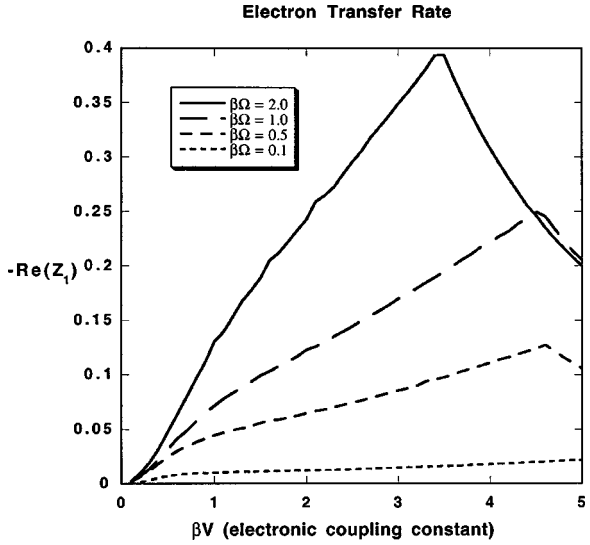

FIG. 4. A plot of electron transfer rate constants with $\beta\lambda=8$ in four different solvents ($\beta\Omega=0.1$, $\beta\Omega=0.5$, $\beta\Omega=1$, and $\beta\Omega=2$).

tronic coupling constant βV for $\beta\lambda=8$ and $\beta\Omega=1$. Here, all time and energy variables are scaled by the thermal energy β and $\hbar$ is taken as unity. In Fig. 3, the long-dashed curve is the Marcus rate computed from Eq. (11), the dashed curve is the diffusion-limited nonadiabatic rate computed from Eq. (14), and the short-dashed curve is the adiabatic diffusion rate computed from Eq. (6) for the adiabatic potential surface given by Eq. (5). The solid curve is the eigenvalue solution, which agrees with the nonadiabatic predictions and crosses over to the adiabatic limit. Unlike the prediction of Eq. (14), the rate constant from the eigensolution does not saturate as the coupling increases but exhibits a transition from nonadiabatic curve crossing to adiabatic barrier crossing. Better results can be obtained in the adiabatic regime by using higher activation barriers. The calculated rate can be approximately reproduced by the connection formula, $1/k=1/k_{\mathrm{ET}}+1/k_D$, if the k_D is computed from $k_D=-Z_1$ on the adiabatic surface and if nonadiabatic effects are taken into full account in k_{ET}.

In Fig. 4, comparison of rate constants in four different solvents ($\beta\Omega=0.1$, $\beta\Omega=0.5$, $\beta\Omega=1$, and $\beta\Omega=2$) confirms that faster solvents yield higher rate constants than slow solvents. However, around $V=4$, which is about the half of the reorganization energy, there is a dramatic drop in the rate constant. From Eq. (5), the barrier on the adiabatic surface disappears when $V=\lambda/2$ and thus the electronic state becomes delocalized as shown in Fig. 1(c).[7] Evidently, the drop in the rate is correlated to the transition from localized to delocalized states. In mixed-valence systems, the coupling constant is on the same scale as the reorganization energy, and this observation suggests that experimentally observed oscillations can be understood from an adiabatic viewpoint.[30,31] Based on this picture, electronic coherence arises from Rabi oscillations between two adiabatic surfaces and decays as a result of inhomogeneous distributions and thermal fluctuations of the Rabi frequency.[11,32]

A complete picture of the localization–delocalization transition emerges from the kinetic spectrum of two-state dynamics. Figure 5 shows the real parts of the first four nonzero eigenvalues as a function of the electronic coupling constant for the same set of parameters used in Fig. 3. The diamonds on the curves represent pairs of complex-conjugate eigenvalues. Clearly, the rate drop coincides with the onset of complex eigenvalue in the first nonzero eigenstates, which indicates that underdamped oscillations can be observed in overdamped solvents as the consequence of electronic coherence. Therefore, the nature of the transition is the crossover of two competing time scales and this observation may have universal implications for kinetic transitions.

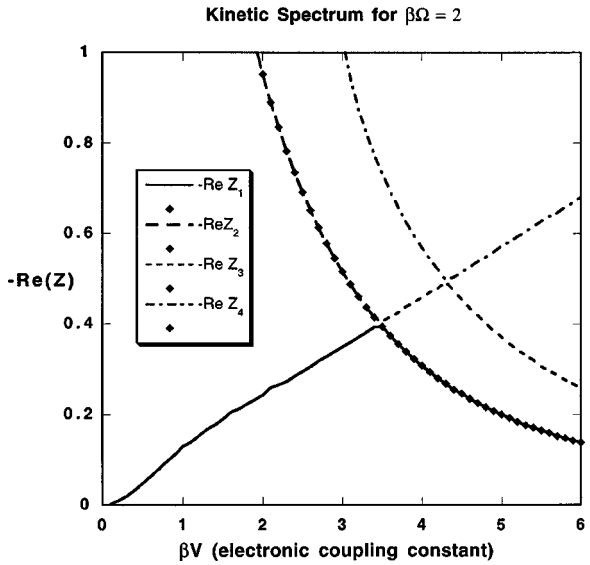

FIG. 5. A plot of the real parts of the first four nonzero eigenvalues ($-\mathcal{R}Z$) as a function of the electronic coupling constant (V) for the same set of parameters used in Fig. 3. The diamonds on the curves represent a pair of complex-conjugate eigenvalues.

More importantly, the set of eigenvalues contains complete information of electron transfer kinetics. For example, on the left half of Fig. 5, the first nonzero eigenstate is well-separated from the higher states, so the single-exponential decay dominates the long-time behavior. When the real parts of two or more eigenvalues are very close, biexponential or multiexponential decay may be observed. Further, complex-conjugate eigenvalues, indicated by the diamonds in Fig. 5, correspond to underdamped oscillations resulting from coherence and dephasing. Detailed calculations reveal complicated kinetic transitions including bifurcation and rotations of eigenvalues in complex plane.

V. CONCLUSION

To summarize, a spectral method has been presented to analyze multiple time scales in electron transfer processes. With the two-state diffusion model, we are able to quantitatively demonstrate the following kinetic behaviors:

(i) The first non-zero eigenvalue recovers Zusman's diffusion-limited nonadiabatic rate in the small coupling limit and Kramers' adiabatic diffusion rate in the large coupling limit. The calculated rate does not saturate as the coupling constant increases, but exhibits a crossover transition from nonadiabatic curve crossing to adiabatic barrier crossing.

(ii) When the electronic coupling constant is about half the reorganization energy, the two lowest nonzero eigensolutions become complex conjugate, indicating underdamped oscillations in overdamped solvents as the consequence of electronic coherence. Thus, the localization–delocalization transition predicted from the lower adiabatic surface is a kinetic transition from incoherent to coherent electron transfer and is the consequence of two competing time-scales.

(iii) In a faster solvent, the rate constant is higher and coherent transfer is more dramatic than in a slower solvent. These observations can be understood as the result of a reduced effective reorganization energy, due to the dynamic nature of the solvent (i.e., the dynamic solvation effect).

(iv) We analyze three possible effects which may cause deviations from equilibrium rate theory: solvent diffusion, adiabatic crossing, and dynamic solvation, and establish domains in parameter space where each of these factors becomes appreciable. In a typical nonadiabatic or weak-adiabatic electron transfer, the Marcus rate theory provides a qualitative description but requires corrections when compared with the experimentally measured rate. In the adiabatic or coherent regimes, the spectral method provides a reliable tool to analyze the kinetics of electron transfer, which cannot be described by the Marcus theory.

Just as eigensolutions to the Schrödinger equation completely determine the dynamics of a quantum system, the eigenstates of the coupled diffusion equations completely characterize the kinetic of a dissipative system. Extensive studies are currently being carried out to investigate electron transfer kinetics in asymmetric two-states, in multistate transfer processes, and in strongly-coupled systems.[33–35] Though presented in the context of electron transfer, this approach is general and can be applied to condensed phase spectroscopy, quantum control of dissipative systems, energy transfer, and other transfer processes.

ACKNOWLEDGMENTS

This work is supported by the Solomon Buchsbaum AT&T Research Fund Award, the Petroleum Research Fund administrated by the American Chemical Society, and an award from Research Corporation. The authors thank Professor Silbey and Professor Oppenheim for interesting discussions. The authors also thank Professor Eric Heller for his insightful comment on the relation between the dynamic solvation effect and spectral line shape.

APPENDIX

For asymmetric electron transfer, we flip the second diabatic surface with respect to the origin, $U_2(E)\rightarrow U_2(-E)$, so that the two-state diffusion equation in Eqs. (10a) and (10b) become

$$\dot{\rho}_1=\mathcal{L}\rho_1-\eta\delta(E-\epsilon)\rho_1+\eta\delta(E+\epsilon)\rho_2, \tag{A1}$$

$$\dot{\rho}_2=\mathcal{L}\rho_2+\eta\delta(E-\epsilon)\rho_1-\eta\delta(E+\epsilon)\rho_2, \tag{A2}$$

where the diffusion operators on the two surfaces are the same, $\mathcal{L}=\mathcal{L}_1$, but the crossing points are different. Next, a new set of density matrices $\rho_1+\rho_2=\rho_+$ and $\rho_1-\rho_2=\rho_-$ are introduced to transform Eqs. (A1) and (A2) into

$$\dot{\rho}_+=\mathcal{L}\rho_+, \tag{A3}$$

$$\dot{\rho}_-=\mathcal{L}\rho_--\eta[\delta(E-\epsilon)-\delta(E+\epsilon)]\rho_+ -\eta[\delta(E-\epsilon)+\delta(E+\epsilon)]\rho_-. \tag{A4}$$

Ignoring the coupling of ρ_+ and ρ_-, we can reduce Eq. (A4) to

$$\dot{\rho}_-\approx\mathcal{L}\rho_--\eta[\delta(E-\epsilon)+\delta(E+\epsilon)]\rho_-, \tag{A5}$$

which is exact for symmetric electron transfer. Then, the same procedure used in deriving Eq. (14) also applies to Eq. (A5), giving

$$k_{\mathrm{ET}}=\frac{k^f_{\mathrm{NA}}+k^b_{\mathrm{NA}}}{1+k^f_{\mathrm{NA}}/k^f_D+k^b_{\mathrm{NA}}/k^b_D}, \tag{A6}$$

where $k^f_{\mathrm{NA}}=\eta\rho(\lambda+\epsilon)$ is the forward rate, $k^b_{\mathrm{NA}}=\eta\rho(\lambda-\epsilon)$ is the backward rate, k^f_D is the forward diffusion rate, and k^b_D is the backward diffusion rate.

[1] R. A. Marcus, J. Chem. Phys. **15**, 155 (1964).
[2] R. A. Marcus and N. Sutin, Biochim. Biophys. Acta **811**, 265 (1985).
[3] H. Frauenfelder and P. G. Wolynes, Science **229**, 337 (1985).
[4] J. E. Straub and B. J. Berne, J. Chem. Phys. **87**, 6111 (1987).
[5] Y. Dakhnovskii, A. A. Ovichinniknov, and M. B. Semenov, Mol. Phys. **63**, 497 (1988).
[6] J. Cao and G. A. Voth, J. Chem. Phys. **106**, 1769 (1997).
[7] D. Chandler, in Liquides, *Cristallisation et Transition Vitreuse, Les Houches, Session LI*, edited by D. Levesque, J. Hansen, and J. Zinn-Justin (Elsevier, New York, 1991).
[8] R. A. Harris and R. Silbey, J. Chem. Phys. **78**, 7330 (1983).
[9] S. Chakravarty and A. J. Leggett, Phys. Rev. Lett. **52**, 5 (1983).

[10] A. J. Leggett, S. Chakravarty, A. T. Dorsey, M. P. A. Fisher, A. Garg, and W. Zwerger, Rev. Mod. Phys. **59**, 1 (1987).
[11] J. Cao, Chem. Phys. Lett. **312**, 606 (1999).
[12] M. D. Newton and N. Sutin, Annu. Rev. Phys. Chem. **35**, 437 (1984).
[13] J. T. Hynes, J. Phys. Chem. **90**, 3701 (1986).
[14] L. D. Zusman, Chem. Phys. **49**, 295 (1980).
[15] R. J. Gordon and S. A. Rice, Annu. Rev. Phys. Chem. **48**, 595 (1997).
[16] S. Mukamel, *The Principles of Nonlinear Optical Spectroscopy* (Oxford, London, 1995).
[17] H. Risken, *The Fokker-Planck Equation* (Springer-Verlag, New York, 1984).
[18] N. G. van Kampen, *Stochastic Processes in Physics and Chemistry* (North-Holland, Amersterdam, 1992).
[19] D. Y. Yang and R. I. Cukier, J. Chem. Phys. **91**, 281 (1989).
[20] A. Garg, J. N. Onuchic, and V. Ambegaokar, J. Chem. Phys. **83**, 4491 (1985).
[21] P. Hanggi, P. Talkner, and M. Borkovec, Rev. Mod. Phys. **62**, 251 (1990).
[22] Y. Dakhnovskii and A. A. Ovchinnikov, Chem. Phys. **80**, 17 (1983).
[23] Y. Jung, J. Cao, and R. J. Silbey (unpublished).
[24] J. Goldstone, Proc. R. Soc. London, Ser. A **239**, 267 (1957).
[25] M. Sparpaglione and S. Mukamel, J. Chem. Phys. **88**, 3263 (1988).
[26] M. Morillo, R. I. Cukier, and M. Tij, Physica A **179**, 411 (1991).
[27] D. R. Reichman and R. J. Silbey, J. Chem. Phys. **104**, 1506 (1996).
[28] J. Cao, J. Chem. Phys. (to be published).
[29] D. B. Matyushov and B. M. Ladanyi, J. Chem. Phys. **110**, 994 (1999).
[30] A. Lucke, C. H. Mak, R. Egger, J. Ankerhold, J. Stockburger, and H. Grabert, J. Chem. Phys. **107**, 8397 (1997).
[31] D. G. Evans, A. Nitzan, and M. A. Ratner, J. Chem. Phys. **108**, 6387 (1997).
[32] Y. Jung, R. J. Silbey, and J. Cao, J. Phys. Chem. A **103**, 9460 (1999).
[33] V. Mujica, M. Kemp, and M. A. Ratner, J. Chem. Phys. **101**, 6849 (1994).
[34] K. Drukker, S. W. de Leeuw, and S. Hammes-Schiffer, J. Chem. Phys. **108**, 6799 (1998).
[35] L. D. Zusman and D. N. Beratan, J. Chem. Phys. **110**, 10468 (1999).